NUMERICAL ANALYSIS OF THE RF FIELD IN A DRIFT TUBE LOADED CAVITY*

K. Batchelor,† T. Nishikawa,‡ and T. Werntz
Brookhaven National Laboratory
Upton, New York

Introduction

The proposed AGS Conversion Program[1] requires accelerated peak beam currents in excess of 100 mA from the 200-MeV injector linac. With this high accelerated current the dispersive properties of the accelerating structure play an important role in determining the quality of the accelerated beam, since the phase and amplitude transients resulting from the RF pulse applied to compensate for the beam load are directly related to these properties. The Alvarez structure has a good bandwidth which may be enhanced by use of multiple stems[2] and the transient and steady state field variation with cavity length may be reduced by the use of multiple feed points. Both of these effects are investigated in this report.

Dispersion Relations for the Multistem Cavity

In a recent paper[2] Giordano and Hannwacker have measured and discussed a set of modes associated with resonance in the circumferential fields of the stem system. These modes, denoted $TS(N)_{10\ell}$, couple to the usual $TM_{01\ell}$ modes and lead to the shaping of the dispersion curve about the TM_{010} resonance. Note that these are the same type of modes discussed by Carne et al. in the treatment of the crossbar structure.[3] In this report the coupled dispersion curves for TS and TM modes are considered in terms of an equivalent circuit for the multistem structure. It has been shown[4] that the lumped circuit constants determined from the measurement of Giordano and Hannwacker have a reasonable N-dependence for N = 1, 2, 3 and 4 stem structures.

Equivalent Circuit

An equivalent circuit for the normal drift tube structure has been given by Hereward[5] in a report concerning energy propagation along the linac. This circuit has been modified to include transverse stem resonances as shown in Fig. 1. Here the series capacity C, represents gap capacity, and series inductances, $2 \times L/2$ represent the inductance which stores the magnetic energy surrounding the drift tube and gap. Then the resonant frequency of the TM_{010} mode is given by

$$\omega_o^2 = \frac{1}{LC} \quad . \tag{1}$$

Also the shunt capacitor C_s, represents the capacitance between the drift tube and outer cylinder (including stems) and the shunt inductances, $2L_s \times 1/2$ represent the inductance due to the loop consisting of the stems and the outer cylinders. L_s and C_s give the transverse stem resonance. In general the stem-loops associated with a drift tube will couple to those of the adjacent tubes giving a mutual inductance M_s between them. (Note that here the structure differs from the crossbar, where M_s is zero due to the rotation of alternate bars by 90°, but where there is mutual coupling between alternate sets of bars.) It will become evident later that the resonant frequency of the $TS(N)_{100}$ mode is given by

$$\omega_s^2 = \frac{1}{L_s C_s} \times \frac{2L_s}{2L_s + M_s} \quad . \tag{2}$$

Let V be the potential between the drift tube and ground (outer cylinder) and I the current from left to right through the drift tubes and gaps, and, further, we write the shunt current from drift tube center to ground as i and divide it into three components i_1, i_2 and i_3, corresponding to three shunt elements, $2L_s$, C_s and $2L_s$ respectively. Then from Floquet's theorem for the periodic structure, the voltages and currents are all multiplied by $e^{j\varphi}$ when we move down the structure by one period. φ is the cell-to-cell phase shift and is given by kL_o, where k is the propagation constant and L_o the cell length. The voltages and currents are related by

$$V_o(e^{j\varphi} - 1) = -\left(j\omega L + \frac{1}{j\omega C}\right) I_o \tag{3}$$

$$V_o = 2j\omega L_s\, i_1 + j\omega M_s\, i_3\, e^{-j\varphi} \tag{4}$$

$$= 2j\omega L_s\, i_3 + j\omega M_s\, i_1\, e^{+j\varphi} \tag{4'}$$

$$= \frac{i_2}{j\omega C_s} \quad . \tag{4''}$$

From Eqs. (4), (4′) and (4″) we have

$$i = i_1 + i_2 + i_3 =$$

$$= j\,\frac{C_s}{\omega}\left[\omega^2 - \frac{4L_s}{\left(4L_s^2 - M_s^2\right)C_s}\left(1 - \frac{M_s}{2L_s}\cos\varphi\right)\right] V_o \quad . \tag{5}$$

Since the shunt current is given by $I_o(e^{-j\varphi}-1)$, we can eliminate V_o and I_o from Eqs. (3) and (5) to give the dispersion equation

$$B(1 - \cos\varphi) = \frac{\{\omega^2-\omega_o^2\}\{\omega^2-\omega_s^2\,[1+\varepsilon(1-\cos\varphi)]\}}{\omega^2\,\omega_o\,\omega_s} \tag{6}$$

*Work performed under the auspices of the U.S. Atomic Energy Commission.

†On leave from Rutherford High Energy Laboratory.

‡On leave from Dept. of Physics, University of Tokyo.

where

$$B = 2\sqrt{\frac{C}{L}}\sqrt{\frac{L_s}{C_s}}\sqrt{1+\frac{M_s}{2L_s}} \qquad (7)$$

and

$$\epsilon = \frac{M_s}{2L_s - M_s} \quad . \qquad (8)$$

The behavior of the dispersion curves shows the same types of advantages in reducing beam loading and detuning effect as described by Nishikawa, Giordano and Carter for alternating periodic structures.[6] The dispersion equation has two solutions for $\varphi = 0$ (zero mode), $\omega = \omega_o$ and $\omega = \omega_s$. In general two passbands exist describing TM_{01} and $TS(N)_{10}$ type modes and are separated by a stopband between ω_o and ω_s. For the special case of $\omega_o = \omega_s$, these bands merge to a single passband and give a finite group velocity

$$V_g = \frac{\partial\omega}{\partial k} = \frac{\omega_o L_o}{2}\sqrt{\frac{B}{2}} \quad . \qquad (9)$$

For $\omega_o \neq \omega_s$ the group velocity vanishes and the mode separation between the TM_{010} and TM_{011} modes approximates to

$$\omega_1 - \omega_o \approx \frac{1}{2}\frac{\partial^2\omega}{\partial\varphi^2}\left(\frac{\pi}{n_o}\right)^2 = \frac{\pi^2 B}{4n_o^2}\frac{\omega_o^2\,\omega_s}{\omega_o^2 - \omega_s^2} \qquad (10)$$

where n_o is the total number of cells. Since the separation given by Eq. (10) increases linearly as ω_s approaches ω_o, the advantages of reduced sensitivity to beam loading, tuning errors and other perturbations for a structure which is adjusted to near enough this frequency are assured.

By using measured frequencies for ω_o and ω_s and, in addition, values for the π mode of TS band and the $\pi/2$ mode of the TM band for the one and four stem structures, and the π mode of the TS band and the $\pi/3$ mode of the TM band for the two and three stem cases, it is possible to determine the parameters ω_o, ω_s, B and ϵ, and hence plot the dispersion curves for 1, 2, 3 and 4 stem structures as in Fig. 2. The solid curves show the calculated curves and the points indicated by circles, triangles, squares and crosses are the measured frequencies; those heavily written show the points used for the calculation. The variations of B, ω_s and ϵ with the number of stems N are given in Fig. 3.

Field Excitation

The Alvarez structure used in existing proton linacs utilizes a standing wave configuration in a long cavity which is similar to the TM_{01n} mode in a cylindrical cavity. The field distribution in such a cavity is a complex function of such factors as beam loading, drift tube loading, wall losses and other perturbations. However, it is possible to expand the actual field in terms of the normal modes which form a complete orthogonal set of functions obtained from the field in an ideal cavity. If such a normal mode is well defined and separated from its nearby modes, then normal mode analysis is a useful method by which the various effects caused by interactions or perturbations within the cavity may be examined. In this report both steady state and transient phenomena are studied for a cavity excited by a well-padded generator and with a bunched beam passing along the axis. A more detailed treatment is given in reference 7.

Normal Modes in a Long Cavity

Taking the normal electric field, $E_n(z,r,\theta)$ the actual field may be expressed as

$$\vec{E}_n(z,r,\theta,t) = \sum_n V_n(t)\,\vec{E}_n(z,r,\theta) \quad . \qquad (11)$$

From Maxwell's equations and orthogonal relations, the expansion coefficient of $V_n(t)$ satisfied the equation of forced oscillations,[8]

$$\frac{d^2V_n}{dt^2} + \omega_n^2 V_n =$$

$$= \frac{-\omega_n}{\sqrt{\epsilon\mu}}\int_s(\vec{E}\times\vec{H}_n)\cdot\vec{n}ds + \frac{1}{\epsilon}\frac{d}{dt}\int_s,(\vec{H}\times\vec{E}_n)\cdot\vec{n}ds$$

$$- \frac{1}{\epsilon}\frac{d}{dt}\int_v \vec{J}\cdot\vec{E}_n\,dv \quad . \qquad (12)$$

The first term on the right hand side is integrated over the non-ideal conducting surfaces, S, such as glossy metallic walls of the cavity. By means of the standard evaluation of Q_o from wall losses, this can be rewritten as a damping term,

$$-(1+j)\frac{\omega_n}{Q_o}\cdot\frac{dV_n}{dt} \quad . \qquad (13)$$

The surface integral in the second term is performed over the non-ideal open surface, S', and gives the effect of coupling the cavity to an outside system. One part of this term gives the forced oscillation by an external source and the other additional damping due to circuit losses ($\propto 1/Q_{ext}$). Effects of the beam within the cavity are represented by the last term where the current density $\vec{J}$ at a point is multiplied by the normal electric field at that point and integrated over the cavity volume. Consider first of all a cavity with no beam excited by a well-padded generator, then Eqs. (12) and (13) give

$$\frac{d^2V_n}{dt^2} + (1+jK_n)\frac{\omega_n}{Q_n}\frac{dV_n}{dt} + \omega_n^2 V_n$$

$$= A\,U_n e^{j\omega t} - \frac{\omega_n}{U_n Q_{ext,n}}\sum_{n'\neq n} U_n'\frac{dV_n'}{dt} \qquad (14)$$

where Q_n, $Q_{ext,n}$ and K_n are given by

$$\frac{1}{Q_n} = \frac{1}{Q_{on}} + \frac{1}{Q_{ext,n}} \tag{15}$$

$$\frac{1}{Q_{ext,n}} = \frac{U_n^2}{\epsilon\, \omega_n Z_o} \tag{16}$$

and

$$K_n = \frac{Q_n}{Q_{o,n}} \quad . \tag{17}$$

Z_o is the characteristic impedance of the waveguides in which only one propagating mode is assumed. At the surface, S′, the cavity normal mode field, E_n, is related to the normal tangential component of the waveguide mode $\vec{e}$,

$$\vec{E}_n = U_n \vec{e} \ (U_n \text{ is a real coefficient}). \tag{18}$$

Assuming the ℓ mode resonant frequency to be given by

$$\omega'_\ell = \omega_\ell \left(1 - \frac{1}{2} Q_{o\ell}\right) \tag{19}$$

we may obtain the equation for forced oscillation of the resonant mode (n=ℓ) at resonance as

$$\frac{d^2V_\ell}{dt^2} + (1 + jK_\ell) \frac{\omega_\ell}{Q_\ell} \frac{dV_\ell}{dt} + \omega_\ell^2 V_\ell = A\, U_\ell\, e^{j\omega'_\ell t} \tag{20}$$

and for nonresonant modes ($n \neq \ell$)

$$\frac{d^2V_n}{dt^2} + (1 + jK_n) \frac{\omega_n}{Q_\omega} \cdot \frac{dV_n}{dt} + \omega_n^2 V_n = A\, U_n\, e^{j\omega'_\ell t} - \frac{U_n}{U_\ell} \frac{\omega_\ell}{Q_{ext,\ell}} \frac{dV_\ell}{dt} \quad . \tag{21}$$

These equations can be solved for a step function incident wave (A = 0 for $t \leq 0$ and A = constant for $t > 0$) and $V_n = 0 = \dot{V}_n$ at t = 0, the solution involving terms having angular frequency ω_n representing free oscillations induced by the transient and terms involving ω_ℓ which are forced oscillations for both the transient and steady state. In order to determine the field inside a drift tube cavity it is necessary to assume a proper boundary condition at S′ which leads to an evalution of U_n. If the power is fed from one end of the cavity (z = 0) then the nearby modes have nearly the same normal mode field patterns at S′ as for the resonant mode, so all modes are excited in phase at z = 0. Thus, except for high n's.

$$U_n = \sqrt{2}\, U_o \quad . \tag{22}$$

For a cavity coupled at any other point (z feed) in the cavity the value of U_n will depend on the z dependence of the mode in question and we may write

$$U_n = \sqrt{2}\, U_o \cos \frac{n \pi z \text{ feed}}{L} \quad . \tag{23}$$

Note that this may be in error for a drift tube loaded cavity due to the asymmetric distribution of drift tubes along the cavity axis.

Steady State Field

Assuming that

$$\frac{\omega'_\ell \omega_n}{Q_n} \ll \left|\omega_n'^2 - \omega_\ell'^2\right| \ ,$$

we get the steady state solution of

$$E(z,t) = = E_o e^{j\omega'_o t}\left[1 + 2\, j \frac{\omega_o'^2}{Q_{oo}} \sum_{n \geq 1} \frac{\cos \frac{n\pi z \text{ feed}}{L} \cos \frac{n\pi z}{L}}{\omega_n'^2 - \omega_o'^2}\right] \tag{24}$$

where

$$E_o = \frac{A \mathcal{E}_o U_o}{\sqrt{2}j} \frac{Q_o}{\omega_o'^2}$$

and $\mathcal{E}_o$ is a normalization constant. The first term in the bracket arises from the resonant zero mode, and the others from higher modes. Each higher order mode is 90° out of phase with the resonant mode leading to the phase shift and amplitude change along the length.

Transient Field

In the first order approximation for a transient state the build up curve of the resonant mode (n = 0) is from the solution of Eq. (20).

$$E_o e^{j\omega'_o t}\left(1 - e^{\frac{-\omega'_o t}{2Q_o}}\right) \tag{26}$$

whereas for a nonresonant mode ($n \neq 0$, $n \ll L/Lo$) the term

$$\sqrt{2}\, jE_o \frac{\omega_o'^2}{Q_o\left(\omega_n'^2 - \omega_o'^2\right)} \frac{U_n}{U_o} e^{j\omega'_o t}\left[1 - \frac{Q_o}{Q_{ext,o}}\left(1 - e^{\frac{-\omega'_o t}{2Q_o}}\right) - e^{\frac{-\omega'_n t}{2Q_n}} e^{j(\omega'_n - \omega'_o)t}\right] \cos \frac{n\pi z}{L} \tag{27}$$

is given from the solution of Eq. (21). Equation (27) shows wiggles which arise from the beat between the free oscillations of that mode and the driving force, the angular frequency of the beat beam

$$\Omega_{on} = \omega'_n - \omega'_o \quad . \tag{28}$$

for a cavity coupled at a single point (z feed) we have

$$E(z,t) = E_o e^{j\omega'_o t}\left[X(z,t) + jY(z,t)\right] \tag{29}$$

$$X(z,t) \simeq 1 - e^{\frac{-\omega_o' t}{2Q_o}} - \frac{\omega_o'}{Q_o} \sum_{n\geq 1} \frac{\sin \Omega_{on} t}{\Omega_{on}} e^{-\frac{\omega_n' t}{2Q_n}} \cdot \cos \frac{n\pi\, z_{feed}}{L} \cos \frac{n\pi z}{L} \quad (30)$$

$$Y(z,t) \simeq - \frac{\omega_o'}{Q_o} \left[\sum_{n\geq 1} \frac{\left(1 - e^{\frac{-\omega_n' t}{2Q_n}}, \cos \Omega_{on} t\right)}{\Omega_{on}} \cos \frac{n\pi\, z_{feed}}{L} \cos \frac{n\pi z}{L} - \frac{Q_o}{Q_{ext,0}} \left(1 - e^{\frac{-\omega_o' t}{2Q_o}}\right) \sum_{n\geq 1} \frac{\cos \frac{n\pi\, z_{feed}}{L} \cos \frac{n\pi z}{L}}{\Omega_{on}} \right] . \quad (31)$$

The amplitude and phase of the field are now given by

$$|E(z,t)| = E_o \sqrt{X^2(z,t) + Y^2(z,t)} \quad (32)$$

and

$$\varphi(z,t) = \tan^{-1} \frac{Y(z,t)}{X(z,t)} . \quad (33)$$

Calculated values of X(z,t) and Y(z,t) at the center of the AGS linac, for modes up to TM_{014} are shown in Figs. 4a and 4b respectively. Measured values of frequencies and Q's are used for the computation. Figure 5 shows the calculated phase transient between the center and input of the cavity. This calculation assumes zero coupling to the TM_{011} and TM_{013} modes. In practice the coupling loop is not at the electrical center of the cavity so there is some coupling to these modes resulting in the transient phases between center and ends of the cavity shown in Figs. 6a and 6b. The steady state phase and amplitude variation for these center-fed and near-center-fed cases are shown in Figs. 7a, 7b, 8a and 8b respectively where measured values are also presented.

Multiple Feeds

A reduction of the transient and steady state amplitude and phase variations along the cavity length may be achieved by feeding power into the cavity at more than one point. For example, by feeding in phase at the L/4 and 3L/4 points the resulting summed fields are zero for all modes where $n \neq 0$, up to and including TM_{014} so a considerable reduction in amplitude and phase variation is achieved. Typical results for this case are shown in Figs. 9a and 9b for the transient case and Figs. 10a and 10b for the steady state solution.

Beam Loading in a Drift Tube Accelerator

Nishikawa[7] has shown that the beam loading in a drift tube cavity gives rise to a decrease in field strength on the axis which is given by the relation

$$\Delta E_b(t) \simeq - \frac{r_{eo} I_o \omega_o' f_o \cos \varphi_b}{2Q_{oo} T_o} \cdot t' \quad (34)$$

where I_o = beam current averaged over bunches, φ_b = phase angle at center of beam bunches, T_o = transit time factor, f_o is a form factor given by $\sin \delta\varphi/2 \,/\, \delta\varphi/2$ for a short bunch with a constant phase spread $\delta\varphi$, r_{eo} is the shunt impedance per unit length of the structure, Q_{oo} the unloaded Q value and $t' = t - t_o$ where t_o is time at which the beam starts. If the beam pulse length t_w is less than the build-up time this effect is of a transient nature and gives rise to an almost linear decrease in the accelerating field with time.

To obtain a good energy spectrum it is customary to increase the input beam power during the beam pulse by an amount equal to the beam power. This extra energy may be added as a step function or a ramp function both of which give rise to a transient response in the cavity due to excitation of nonresonant modes ($n \neq 0$). The beam itself gives very small excitation to these higher order modes, so compensation cannot be achieved for these modes. Therefore a phase and amplitude distribution within the beam pulse period results from the addition of the extra beam compensation energy. These phase and amplitude effects will vary with position along the cavity length due to the normal field distributions of the higher order modes. The calculated and measured phase and amplitude shifts between the center and ends of the AGS linac for an optimum compensation pulse are shown in Figs. 11a and 11b, where a 30 mA peak beam current was being accelerated.

Conclusions and Observations

The normal mode analysis of standing wave linacs has been shown to give a good representation of the fields existing inside the resonant cavity. In making the calculations it has been assumed that the presence of drift tubes does not substantially affect the expressions representing the axial components of the normal mode fields. The assumption of a well-padded generator allows the effects of source impedance on the cavity build-up to be neglected. Effects due to a non-uniform beam bunch and space charge effects of a high current beam line have also been neglected. The improved field distribution resulting from a double feed to the cavity has also been demonstrated.

Acknowledgements

The authors would like to thank Dr. John P. Blewett, Dr. George Wheeler and Dr. Arie van Steenbergen for their constant interest in this work. They also are indebted to Mr. S. Giordano for the experimental results from the multi-stem structure.

References

1. "Alternating Gradient Synchrotron Conversion Program - Scope of Phase I", BNL 9500, September 1965.

2. S. Giordano and J.P. Hannwacker, "Measurements on a Multistem Drift Tube Structure", Proc. 1966 Linear Accelerator Conference, Los Alamos, October 3-7, 1966, LA-3609 (CFSTI, Springfield, Virginia), p. 88.

3. A. Carne, G. Dome, N. Fewell and W. Jungst, "Development of the Crossbar Structure for a P.L.A.", Proc. Vth International Accelerator Conference on High Energy Accelerators, Frascati, September 1965 (CNEN, Rome, 1966), p. 624.

4. T. Nishikawa, "Equivalent Circuit and Dispersion Relation for the Multistem Drift Tube Structure", BNL Accelerator Dept. Internal Report AADD-125, November 1966.

5. H.J. Hereward, "Some Examples of Energy Flow in the Alvarez Structure", CERN Internal Report MPS/DL Int. 65-1, 1965.

6. T. Nishikawa, S. Giordano and D. Carter, "Dispersion Relation and Frequency Characteristics of Alternating Periodic Structures for Linear Accelerators", Rev. Sci. Instr. 37, 652 (1966).

7. T. Nishikawa, "Normal Mode Analysis of Standing Wave Linacs - Field Excitation and Beam Loading in Linac Cavities", BNL Accelerator Dept. Internal Report AADD-87, November, 1965.

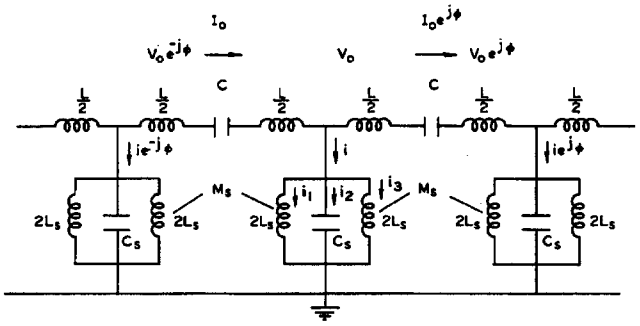

Fig. 1. An equivalent circuit for the multistem drift tube structure.

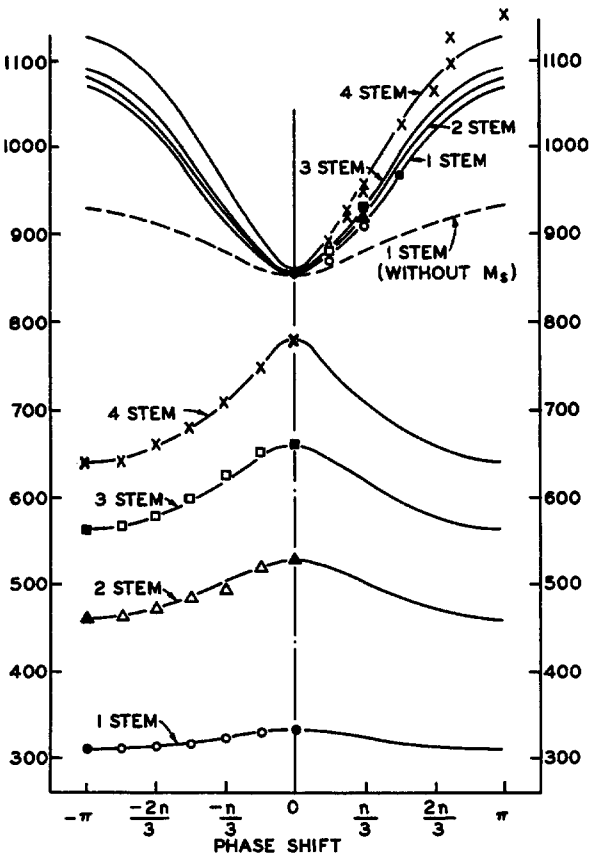

Fig. 2. Comparison between measured and calculated dispersion curves. Pairs of measured frequencies for the same modes of 4 stem cases were obtained by different end terminations.

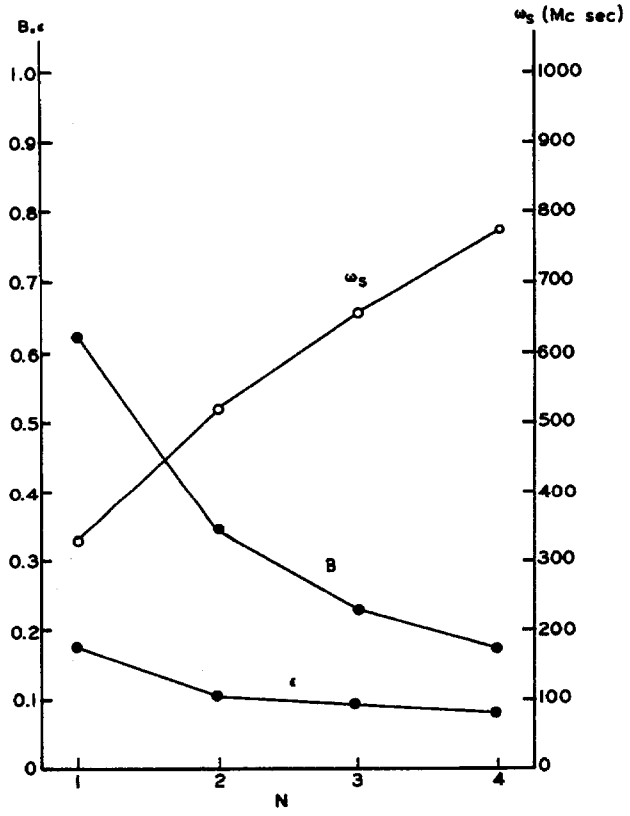

Fig. 3. N-dependence of B, ω_S and ϵ.

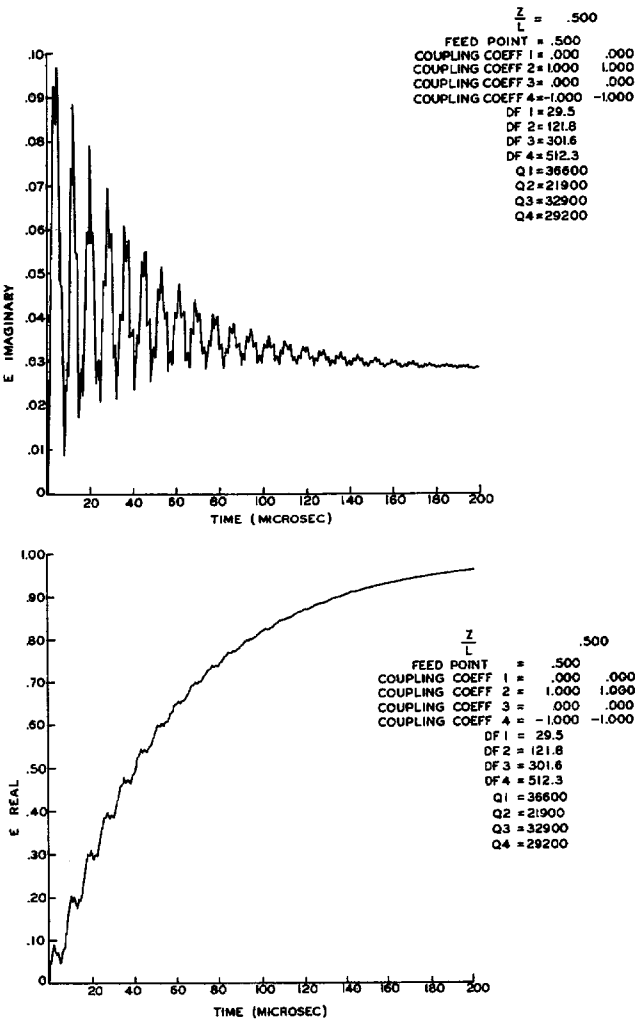

Fig. 4. Calculated values of X(z,t) and Y(z,t) at center of AGS linac.

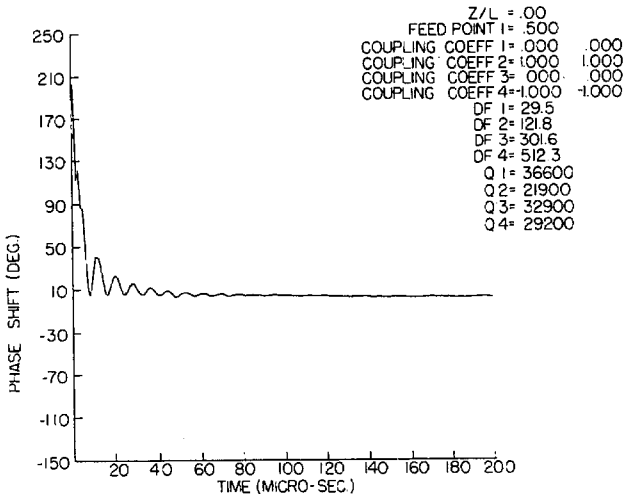

Fig. 5. Transient phase shift between low energy end and center of AGS cavity.

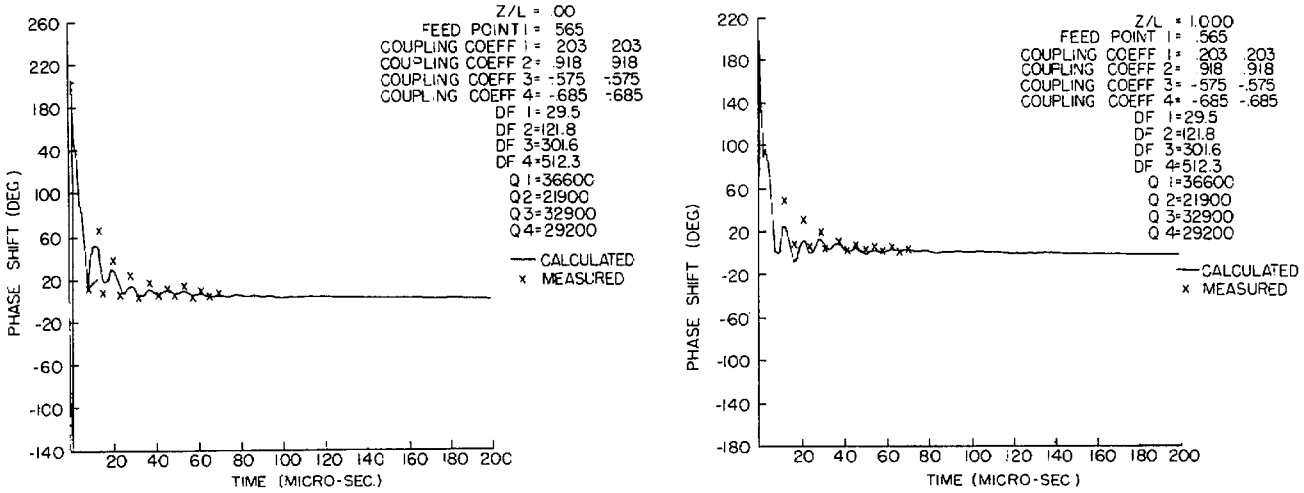

Fig. 6. Transient phase shift between center and both ends of AGS linac.

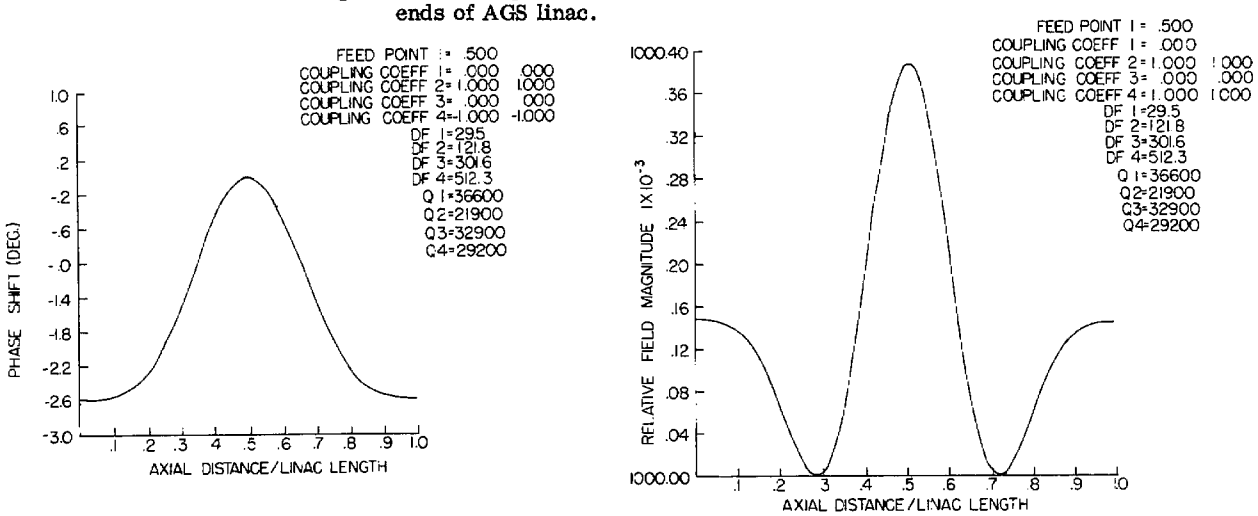

Fig. 7. Steady state phase and amplitude variation along the length of the AGS linac—ideal center feed.

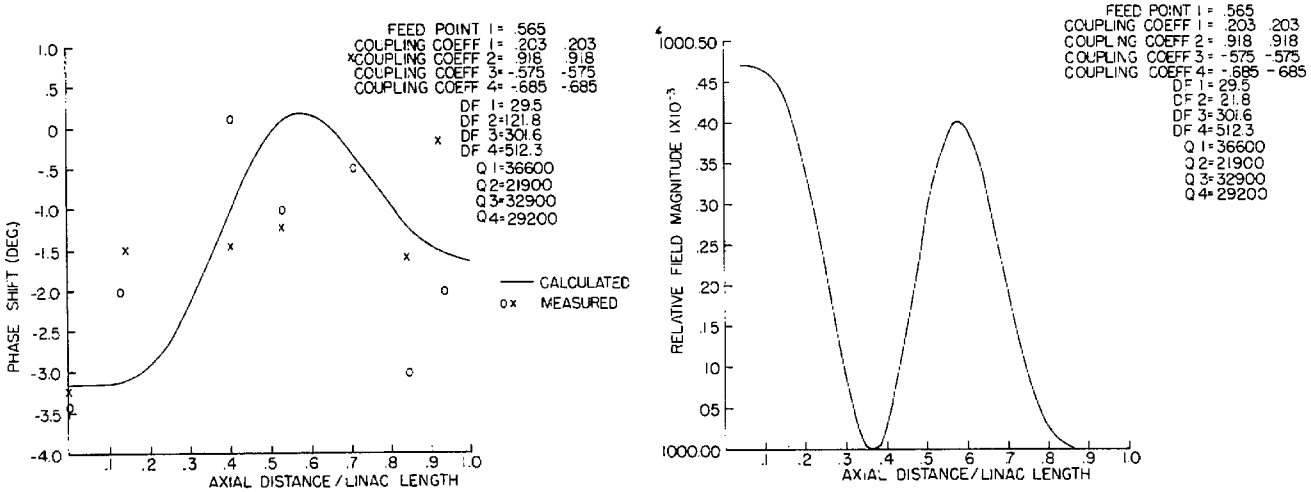

Fig. 8. Steady state phase and amplitude variation along the length of the AGS linac— practical feed position.

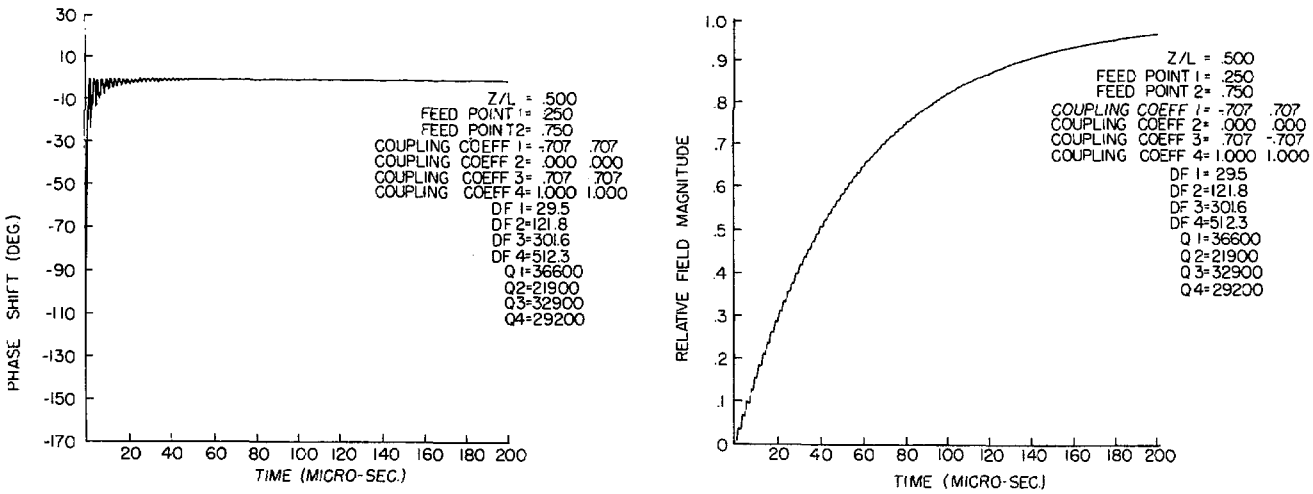

Fig. 9. Transient phase shift between center and ends of the cavity—feeds at L/4 and 3L/4 points.

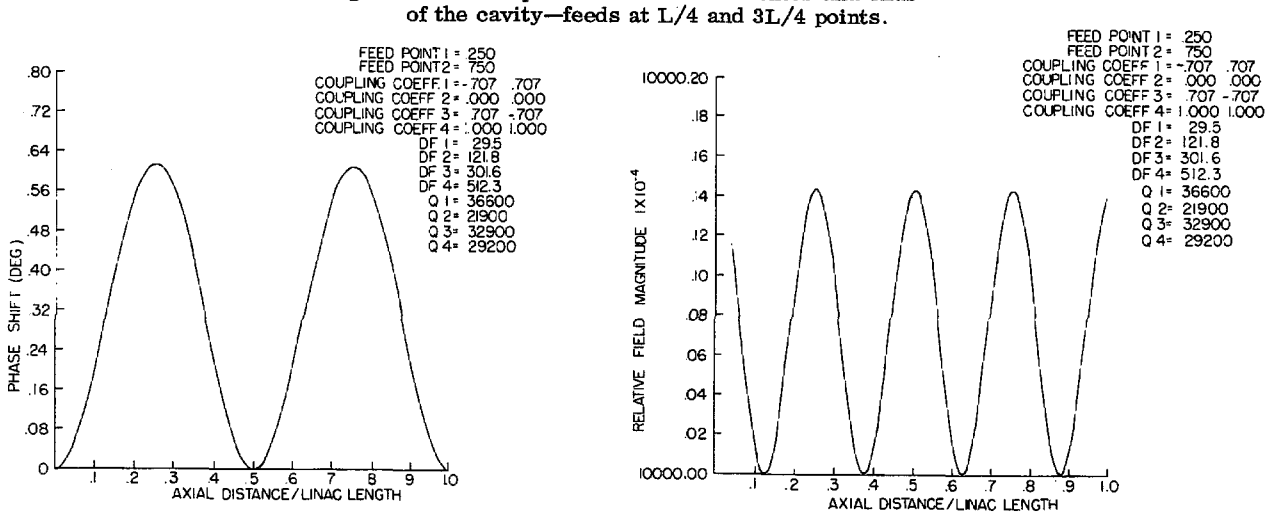

Fig. 10. Steady state phase and amplitude variations along the cavity length—feeds at L/4 and 3L/4 points.

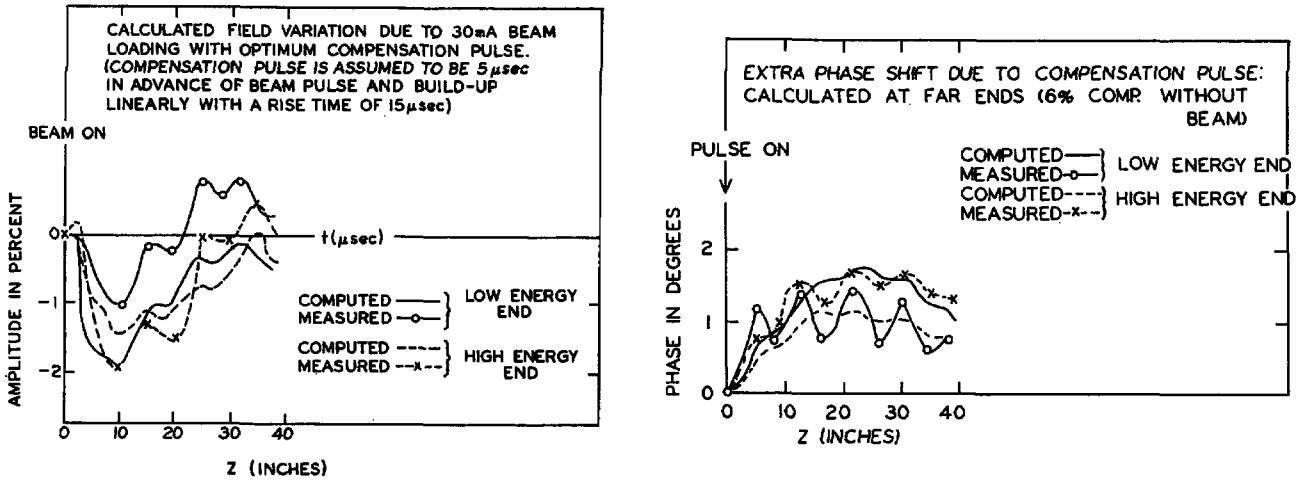

Fig. 11. Calculated and measured phase and amplitude shifts due to the beam compensation pulse.